



The O'KEYPS Equation and 60 Years Beyond

Dan Li¹

Received: 1 July 2020 / Accepted: 28 October 2020
© Springer Nature B.V. 2020

Abstract

Some 60 years ago, six researchers obtained a semi-empirical equation that describes how the stability correction function for the mean velocity profile (ϕ_m) in the atmospheric surface layer varies with the stability parameter—the famous O'KEYPS equation. Their derivations are essentially based on interpolation of the turbulent eddy viscosity between neutral and convective conditions. Comparing the O'KEYPS equation with new theoretical developments—such as phenomenological and cospectral budget models—suggests that Heisenberg's eddy viscosity provides a unifying framework for interpreting the behaviour of ϕ_m . The empirical coefficient in the O'KEYPS equation, which is on the order of 10 based on data fitting to observations, is found to be primarily linked to the increase of the size of turbulent eddies as instability increases. The ratio of the sizes of turbulent eddies under convective and neutral conditions is on the order of $1/\kappa$, where κ is the von Kármán constant, and is modulated by the turbulent Prandtl number.

Keywords Heisenberg's eddy viscosity · Mean velocity profile · O'KEYPS equation · Stability correction function · Turbulent Prandtl number

1 Introduction

In an idealized atmospheric surface layer where Monin–Obukhov similarity theory applies (Monin and Obukhov 1954), the vertical gradient of mean flow velocity (dU/dz), when normalized by the friction velocity ($u_* = \sqrt{\tau/\rho}$, where τ is the surface stress and ρ is the air density) and the height (z) above the ground (or above the displacement height for canopies), is only a function of the so-called stability parameter ζ

$$\phi_m(\zeta) = \frac{\kappa z}{u_*} \frac{dU}{dz}, \quad (1)$$

where κ is the von Kármán constant. The stability parameter $\zeta = -\frac{(g/\Theta)(\overline{w'\theta'})_s}{u_*^2/(\kappa z)}$ characterizes the ratio of buoyant production (or destruction) and mechanical production rates of turbulence kinetic energy (TKE) (Stull 1988; Garratt 1994; Kaimal and Finnigan 1994), where g is the

✉ Dan Li
lidan@bu.edu

¹ Department of Earth and Environment, Boston University, Boston, MA, USA

acceleration due to gravity ($= 9.81 \text{ m s}^{-2}$), Θ is the mean virtual potential temperature, $(\overline{w'\theta'})_s$ is the surface buoyancy flux. Hereafter the overbar indicates the Reynolds average and the primes indicate deviations from the Reynolds averages. Under neutrally stratified conditions (i.e., when there is no buoyancy effect or $\zeta = 0$), $\phi_m(0) = 1$ and the above equation recovers the classic logarithmic mean velocity profile. As a result, $\phi_m(\zeta)$ is often called the stability correction function for the mean velocity profile as it accounts for distortions to the logarithmic mean velocity profile by buoyancy effects.

The above equation can be reorganized as follows

$$u_*^2 = \frac{\kappa z u_*}{\phi_m(\zeta)} \frac{dU}{dz}. \quad (2)$$

This implies that the turbulent shear stress (u_*^2) is proportional to the vertical gradient of the mean velocity and the proportionality coefficient, called the turbulent or eddy viscosity (K_m) and representing the capacity of turbulence in transporting momentum, is $\kappa z u_*/\phi_m(\zeta)$. Denoting $K_m^{\text{neu}} = \kappa z u_*$, the eddy viscosity under neutral conditions, leads to $K_m = K_m^{\text{neu}}/\phi_m(\zeta)$, which suggests that the stability correction function $\phi_m(\zeta)$ modulates the magnitude of K_m relative to its neutral counterpart. The eddy viscosity under neutral conditions ($K_m^{\text{neu}} = \kappa z u_*$) is constrained by dimensional homogeneity, namely, the dimension of eddy viscosity must be a velocity scale multiplied by a length scale, the latter of which is often interpreted using Prandtl's mixing-length concept (Stull 1988; Garratt 1994; Kaimal and Finnigan 1994).

Knowing the exact behaviour of $\phi_m(\zeta)$ is the prerequisite to computing the turbulent shear stress from the mean velocity profile in observations and simulations. Unfortunately, Monin–Obukhov similarity theory, which is based on dimensional analysis, cannot predict the exact shape of $\phi_m(\zeta)$. Under unstable conditions (when $\zeta < 0$), which is the focus here, both buoyancy and shear generate TKE. One would expect that the eddy viscosity is enhanced when compared to K_m^{neu} due to the extra TKE generated by the buoyancy force, which would then imply a smaller value of $\phi_m(\zeta)$ for $\zeta < 0$ compared to $\phi_m(0) = 1$. As ζ becomes more negative, $\phi_m(\zeta)$ should further decrease. This is well observed in field experiments (see Höglström 1988, 1996 for reviews) and reproduced by large-eddy simulations and direct numerical simulations (Khanna and Brasseur 1997; Maronga and Reuder 2017; McColl et al. 2017; Pirozzoli et al. 2017; Li et al. 2018b).

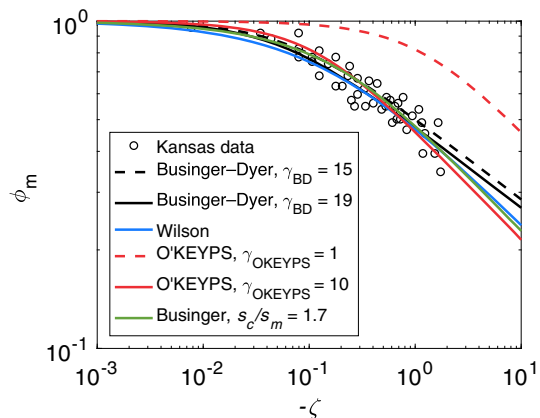
In fact, many empirical functions have been proposed to describe ϕ_m , of which the most widely used is the Businger–Dyer relation (Dyer and Hicks 1970; Businger et al. 1971; Dyer 1974; Businger 1988). The Businger–Dyer relation under unstable conditions is expressed as

$$\phi_m(\zeta) = (1 - \gamma_{\text{BD}}\zeta)^{-1/4}, \quad (3)$$

where γ_{BD} is an empirical coefficient determined from data fitting. Using observations collected during the Kansas experiment, Businger et al. (1971) obtained a value of 15 with $\kappa = 0.35$. The use of $\kappa = 0.4$, which is more popular in the current literature, slightly modifies the value of γ_{BD} to be 19 (Höglström 1988), but the difference is rather minor (see Fig. 1). As can be seen from Eq. 3, the Businger–Dyer relation yields a $-1/4$ power-law scaling for ϕ_m under convective conditions (i.e., when $-\zeta \gg 1$). But there have been theoretical arguments, as will be seen shortly, suggesting that ϕ_m should behave like $(-\zeta)^{-1/3}$ under convective conditions. One empirical function that recovers this $-1/3$ scaling for $-\zeta \gg 1$ was proposed by Wilson (2001)

$$\phi_m(\zeta) = [1 + 3.59(-\zeta)^{2/3}]^{-1/2}. \quad (4)$$

Fig. 1 The stability correction function ϕ_m . The circles are data from the Kansas experiment. The black dash line and the black line are the Businger–Dyer relations with $\gamma_{BD} = 15$ and $\gamma_{BD} = 19$, respectively. The blue line is the Wilson formulation. The red dashed line and the red line are the solutions of the O'KEYPS equation with $\gamma_{OKEYPS} = 1$ and $\gamma_{OKEYPS} = 10$, respectively. The green line is Businger's model (Eq. 17)



It can be seen from Fig. 1 that the Wilson formulation only starts to deviate from the Businger–Dyer relation when $-\zeta > 1$. Unfortunately, it remains unclear which formulation is better supported by observations due to the lack of data for $-\zeta > 1$. Other empirical functions can be also found in the literature (Högström 1988, 1996), but the general shape is similar to the Businger–Dyer relation and the Wilson formulation.

On the theory (or semi-empirical theory, to be more accurate) side, early attempts in the late 1950s to early 1960s to explain the behaviour of ϕ_m over a range of stabilities led to the famous O'KEYPS equation (named after Obukhov, Kazansky, Ellison, Yamamoto, Panofsky, and Sellers) (Lumley and Panofsky 1964; Businger and Yaglom 1971)

$$\phi_m^4 - \gamma_{OKEYPS} \phi_m^3 \zeta = 1, \quad (5)$$

where γ_{OKEYPS} is an empirical coefficient that needs to be determined through data fitting. The values of γ_{OKEYPS} vary among different studies. The two extremes were suggested by Ellison (1957) (6.67–7.14) and Yamamoto (1959) (41.2–70.1). Later, Panofsky et al. (1960) suggested 13.8. Note that the often quoted value of 18 from Panofsky et al. (1960) is actually γ_{OKEYPS}/Pr_t , where Pr_t is the turbulent Prandtl number assumed to be a constant of $1/1.3 = 0.77$ in their paper. For an illustration, the ϕ_m predicted by the O'KEYPS equation with $\gamma_{OKEYPS} = 10$ is shown in Fig. 1. The O'KEYPS equation suggests a $-1/3$ scaling for ϕ_m in the convective limit. This can be easily seen from Eq. 5: when $-\zeta \gg 1$, the second term on the left-hand side of Eq. 5 becomes much larger than the first term, yielding $\phi_m \sim (-\zeta)^{-1/3}$.

Recent field experiments (Song et al. 2010; Liu et al. 2016) and simulations (Khanna and Brasseur 1997; Maronga and Reuder 2017; McColl et al. 2017; Pirozzoli et al. 2017; Li et al. 2018b) continue to confirm the general shape of ϕ_m in unstable conditions (and also in mildly stable conditions). More importantly, they provide new information about turbulence properties that was not available when the O'KEYPS equation was derived. It is well established now that the structure of turbulent eddies in the atmospheric surface layer is significantly modified by the buoyancy force (Li and Bou-Zeid 2011; Hutchins et al. 2012; Katul 2019). Studies have shown that the low-frequency ranges of velocity and scalar spectra respond to atmospheric stability effects (Lumley and Panofsky 1964; Kaimal and Finnigan 1994), leading to larger integral length scales with increasing instability (Salesky et al. 2013). The inclination angle of large-scale motions increases as the atmospheric surface layer becomes more unstable (Chauhan et al. 2013; Liu et al. 2017; Salesky and Anderson 2020). The vorticity field also experiences significant changes (Hommema and Adrian 2003;

Carper and Porté-Agel 2004), which might be linked to a potential change of turbulence topology from roll structure (Etling and Brown 1993) to cellular structure (Wyngaard 1985; Schmidt and Schumann 1989) as demonstrated in large-eddy simulations (Shah and Bou-Zeid 2014; Patton et al. 2016; Salesky et al. 2017; Salesky and Anderson 2018). These developments in field experiments and simulations have motivated, and provided empirical support for, various phenomenological theories and cospectral models for the mean velocity and scalar concentration profiles in turbulent boundary layers (Gioia et al. 2010; Katul et al. 2011; Salesky et al. 2013; Katul et al. 2013a,b; Katul and Manes 2014; Katul et al. 2014; Li et al. 2016b), as well as many other aspects of turbulent flows (see Ali and Dey 2018 and Katul et al. 2019 for recent reviews) over the past decade.

The aim of this study is not to propose a new explanation for the observed behaviour of ϕ_m . Instead, by comparing different attempts to explain ϕ_m , the key controls of the behaviour of ϕ_m under unstable conditions are identified. To begin, the original derivations of O'KEYPS equation and their extensions are reviewed. More recent developments based on phenomenological considerations and cospectral budgets are then discussed. New observational data are also presented to support the generalization.

2 Derivations of the O'KEYPS Equation

While the six researchers derived the O'KEYPS equation differently, one common assumption is that the eddy viscosity in the convective limit does not approach zero and is proportional to the eddy diffusivity, its counterpart for turbulent heat transfer. Namely, the turbulent Prandtl number (Pr_t), or the ratio of eddy viscosity to the eddy diffusivity for heat, remains finite in the convective limit. With this key assumption, the gist of deriving the O'KEYPS equation is to design an eddy viscosity that interpolates between two limits: the neutral limit ($K_m^{\text{neu}} = \kappa z u_*$) and the convective limit ($K_m^{\text{con}} = Pr_t^{\text{con}} K_h^{\text{con}}$), where Pr_t^{con} is the turbulent Prandtl number in the convective limit and K_h^{con} is the eddy diffusivity for heat in the convective limit. The eddy diffusivity for heat in the convective limit (K_h^{con}) has been known since the work of Prandtl (1932) and Priestley (1954, 1955, 1957, 1959)

$$K_m^{\text{con}} = Pr_t^{\text{con}} K_h^{\text{con}} = Pr_t^{\text{con}} c^{\text{con}} \left(\frac{g}{\Theta} \overline{w' \theta'} \right)^{1/3} z^{4/3} = Pr_t^{\text{con}} c^{\text{con}} w_* z, \quad (6)$$

where c^{con} is an empirical coefficient that is on the order of unity and $w_* = \left(\frac{g}{\Theta} \overline{w' \theta'} z \right)^{1/3}$ is the local convective velocity. It can be shown that $w_*/u_* \propto (-\zeta)^{1/3}$. In the derivations of this paper, a dry atmosphere is assumed so that buoyancy is represented by potential temperature instead of virtual potential temperature.

There are two main ways of performing this interpolation. The first method was implicitly used by Ellison (1957) and explicitly stated by Sellers (1962). Heuristic arguments supporting this method can be found in Obukhov (1946), the English translation of can be found in Obukhov (1971), and also in Fleagle and Businger (1981). The second method, based on Heisenberg's eddy viscosity (Heisenberg 1948) and a local equilibrium assumption for the TKE equation, was used by Kazansky and Monin (1956, 1958), Yamamoto (1959), and Panofsky (1961). Other ways of performing the interpolation were also used, but they either do not produce a final result that resembles the O'KEYPS equation or do not have strong physical justification. Those are not discussed here, but readers are referred to Monin and Yaglom (1971).

2.1 A Constant Turbulent Prandtl Number

The two limits for K_m just discussed, while straightforward to understand, require a priori knowledge of the turbulent fluxes themselves. For example, K_m^{neu} depends on the turbulent momentum flux while K_m^{con} depends on the turbulent heat flux. To avoid the use of fluxes, the eddy viscosities can be reorganized as

$$K_m^{\text{neu}} = (\kappa z) \frac{dU}{dz}, \quad (7)$$

$$K_m^{\text{con}} = Pr_t^{\text{con}} (c^{\text{con}})^{3/2} \left(\frac{g}{\Theta} \frac{d\Theta}{dz} \right)^{1/2} z^2. \quad (8)$$

With these two new expressions for K_m^{neu} and K_m^{con} that only involve mean velocity and potential temperature profiles, the next step is to provide a smooth transition between them. The following formulation was provided by Sellers (1962), which was implicitly used by Ellison (1957)

$$K_m^2 = (K_m^{\text{neu}})^2 + (K_m^{\text{con}})^2. \quad (9)$$

This equation reflects the fact that the TKE is generated by both shear and buoyancy forces under unstable conditions, thus K_m is larger than the two limits when the TKE is only produced by shear (the neutral limit) or buoyancy (the convective limit) (Obukhov 1971; Fleagle and Businger 1981). Substituting Eqs. 7 and 8 into Eq. 9 yields

$$\phi_m^4 - \frac{(Pr_t^{\text{con}})^2 (c^{\text{con}})^3 Pr_t}{\kappa^4} \phi_m^3 \zeta = 1. \quad (10)$$

Comparing this to the O'KEYPS equation reveals

$$\gamma_{\text{OKEYPS}} = \frac{(Pr_t^{\text{con}})^2 (c^{\text{con}})^3 Pr_t}{\kappa^4}. \quad (11)$$

A positive γ_{OKEYPS} thus implies a non-zero Pr_t^{con} . The previously discussed $-1/3$ scaling of ϕ_m in the convective limit hinges on a non-zero value of γ_{OKEYPS} . Hence one can argue that the $-1/3$ scaling of ϕ_m in the convective limit predicted by the O'KEYPS equation is in fact a result of assuming a non-zero Pr_t^{con} . More importantly, a constant γ_{OKEYPS} is equivalent to assuming a constant Pr_t throughout the entire unstable regime. However, there is enough evidence showing that this is not the case (Li 2019). With this caveat in mind, which will be revisited later, it is simply pointed out that assuming a constant $Pr_t = 0.7$, with $c^{\text{con}} = 1$, would yield $\gamma_{\text{OKEYPS}} = 13.4$, which is consistent with the values obtained through data fitting.

2.2 The Dissipation Rate of Turbulence Kinetic Energy

Another way of interpolating the eddy viscosity between the neutral and convective limits is to invoke Heisenberg's eddy viscosity (Heisenberg 1948), supplemented by a local equilibrium assumption for the TKE equation (Stull 1988; Garratt 1994; Kaimal and Finnigan 1994), which connects the dissipation rate for the TKE (ϵ) to the production rate

$$\epsilon \approx u_*^2 \frac{dU}{dz} + \frac{g}{\Theta} \overline{w'\theta'}. \quad (12)$$

In the neutral limit, $\epsilon^{\text{neu}} \approx u_*^3/(\kappa z)$, and in the convective limit, $\epsilon^{\text{con}} \approx \frac{g}{\Theta} \overline{w'\theta'}$. Connecting these expressions to the two eddy viscosities presented earlier, one can immediately see that

$K_m^{\text{neu}} \propto (\epsilon^{\text{neu}})^{1/3} z^{4/3}$ and $K_m^{\text{con}} \propto (\epsilon^{\text{con}})^{1/3} z^{4/3}$. Therefore, a natural way to link the two limits is $K_m \propto \epsilon^{1/3} z^{4/3}$, or

$$K_m = A \left(u_*^2 \frac{dU}{dz} + \frac{g}{\Theta} \overline{w'\theta'} \right)^{1/3} z^{4/3} = \frac{A}{\kappa^{1/3}} u_* z (\phi_m - \zeta)^{1/3}. \quad (13)$$

Here, a coefficient A is introduced to recover the neutral limit of ϕ_m . Equation 13, combined with $K_m = \kappa u_* z / \phi_m$, immediately leads to the O'KEYPS equation with $\gamma_{\text{OKEYPS}} = 1$, and the fact that $\phi_m(0) = 1$ yields $A = \kappa^{4/3}$.

From Fig. 1 one can clearly see that the ϕ_m resulting from the O'KEYPS equation with $\gamma_{\text{OKEYPS}} = 1$ does not follow the data and deviates strongly from the well-established empirical functions. To alleviate this problem, another coefficient, B , is introduced

$$K_m = A \left(u_*^2 \frac{dU}{dz} + B \frac{g}{2} \overline{w'\theta'} \right)^{1/3} z^{4/3} = \frac{A}{\kappa^{1/3}} u_* z (\phi_m - B\zeta)^{1/3}. \quad (14)$$

Equation 14 leads to the O'KEYPS equation with $\gamma_{\text{OKEYPS}} = B$ and the fact that $\phi_m(0) = 1$ again yields $A = \kappa^{4/3}$.

This is essentially the derivation of Yamamoto (1959) and Panofsky (1961). The linkage between the eddy viscosity and the dissipation rate of TKE dates back to Heisenberg (1948). The empiricism of this approach lies in the introduction of B in Eq. 14, which is essentially γ_{OKEYPS} and thus has to be on the order of 10 to capture the observed ϕ_m . Yamamoto (1959) interpreted B as the contribution from the other terms in the TKE equation, especially the turbulent transport term. However, this means that the turbulent transport term has to be proportional to $-\zeta$ and an order of magnitude larger, which is not supported by the Kansas experiment (Wyngaard and Coté 1971) and other datasets (Salesky et al. 2013; Li et al. 2016b). In addition, Wyngaard (1984) argued that the use of the eddy viscosity concept implicitly requires local equilibrium in the TKE and turbulent flux budget equations, which would be violated if the turbulent transport term were an order of magnitude larger than the buoyancy term. On the other hand, Panofsky (1961) interpreted B as an empirical indication of the higher efficiency of convectively-driven turbulence in accomplishing vertical transport than shear-driven turbulence.

It should be noted that this derivation still implicitly assumes that the eddy viscosity is proportional to its counterpart for heat transfer in the convective limit and hence the turbulent Prandtl number in the convective limit is non-zero. However, this derivation does not assume a constant turbulent Prandtl number throughout the entire unstable regime.

2.3 Summary

Comparing the above two derivations of the O'KEYPS equation reveals that in the first derivation, a value of γ_{OKEYPS} on the order of 10 explicitly shows up in the final equation but the derivation assumes a constant Pr_t throughout the entire unstable regime. On the other hand, the second derivation does not need to assume a constant Pr_t under unstable conditions, but some empirical coefficient (B) has to be introduced in the budget equation for the TKE. Consequently, most common criticisms of these two derivations are: (1) the assumption of a constant Pr_t in the first derivation, and (2) the introduction of the empirical coefficient (B) in the second derivation.

Later extensions of the O'KEYPS equation mostly focus on the second derivation with two different approaches: (1) proposing a physical justification of γ_{OKEYPS} , or (2) introducing a stability-dependent length scale in the eddy viscosity. The first approach was taken

by Businger (1961) using a TKE spectrum model and the second approach was taken by Yokoyama (1962), Takeuchi and Yokoyama (1963), Herbert and Panhans (1979), and Sander (2000). As will be seen, the two different extensions in fact lead to the same key finding.

In the following, these two different approaches of extending the O'KEYPS equation are first reviewed. Then new developments along the same lines as these extensions are discussed and observational data are presented to support the generalization. After that, the first derivation is revisited by introducing a stability-dependent Pr_t .

3 Extensions of the O'KEYPS Equation

3.1 Businger's Model

As mentioned earlier, Panofsky (1961) interpreted the value of γ_{OKEYPS} as an empirical indication of the higher efficiency of convectively-driven turbulence in producing momentum flux than shear-driven turbulence. Businger (1961) developed a spectrum-based model to demonstrate this. He assumed that turbulence is isotropic once a spectrum is established. The TKE generated by convective turbulence enters the spectrum at a lower wavenumber $k_c = 1/s_c$ than its counterpart generated by shear turbulence, which is at $k_m = 1/s_m$, where s_c and s_m are the corresponding length scales (see Fig. 2a). He further assumed that between k_c and k_m , the energy cascade process only receives the TKE generated by convective turbulence and thus the dissipation rate is simply $\epsilon^{\text{con}} = \frac{g}{\Theta} \overline{w'\theta'}$; however, between k_m and $k = \infty$, the energy cascade process receives the TKE generated by both convectively-driven and shear-driven turbulence and thus the dissipation rate is ϵ (Eq. 12). This yields

$$\begin{aligned} \int_0^\infty E(k) dk &= \int_{k_c}^{k_m} E(k) dk + \int_{k_m}^\infty E(k) dk \\ &= \int_{k_c}^{k_m} c_o (\epsilon^{\text{con}})^{\frac{2}{3}} k^{-\frac{5}{3}} dk + \int_{k_m}^\infty c_o \epsilon^{\frac{2}{3}} k^{-\frac{5}{3}} dk, \end{aligned} \quad (15)$$

where c_o is the Kolmogorov constant (≈ 1.5) (Kolmogorov 1941). He further assumed that the eddy viscosity is proportional to the TKE and the inverse of the wavenumber, namely,

$$K_m^2 = A' \left[\int_0^\infty \frac{E(k)}{k^2} dk \right] = A' \int_{k_c}^{k_m} c_o (\epsilon^{\text{con}})^{\frac{2}{3}} k^{-\frac{11}{3}} dk + A' \int_{k_m}^\infty c_o \epsilon^{\frac{2}{3}} k^{-\frac{11}{3}} dk, \quad (16)$$

where A' is a proportionality coefficient that again can be determined by imposing $\phi_m(0) = 1$. This, combined with $K_m = \kappa u_* z / \phi_m$, yields

$$\phi_m^4 \left[\left(1 - \frac{\zeta}{\phi_m} \right)^{2/3} + \alpha' \left(-\frac{\zeta}{\phi_m} \right)^{2/3} \right]^{3/2} = 1, \quad (17)$$

where $\alpha' = (k_m/k_c)^{8/3} - 1 = (s_c/s_m)^{8/3} - 1$.

This equation is not exactly the same as the O'KEYPS equation but the coefficient α' plays a similar role as γ_{OKEYPS} . Businger (1961) showed that with $s_c/s_m = 1.7$, which corresponds to $\alpha' = 3.1$, Eq. 17 yields good agreement with observational data (see Fig. 1). This implies that the value of γ_{OKEYPS} is related to the ratio s_c/s_m , which characterizes the separation of the length scales at which buoyancy and shear affect the TKE spectrum.

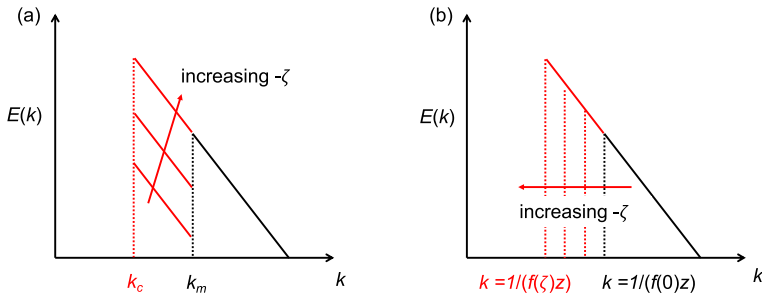


Fig. 2 A spectral view of **a** Businger's model and **b** the cospectral budget model (also the phenomenological model); $E(k)$ is the energy spectrum and k is the wavenumber

3.2 A Stability-Dependent Length Scale

In a nutshell, the derivations by Yokoyama (1962), Takeuchi and Yokoyama (1963), Herbert and Panhans (1979), and Sander (2000) considered the impact of atmospheric instability on the length scale. Instead of using $K_m \propto \epsilon^{1/3} z^{4/3}$, they used $K_m \propto \epsilon^{1/3} s^{4/3} \propto \epsilon^{1/3} z^{4/3} (s/z)^{4/3}$, where s is a new length scale that is assumed to, after normalized by z , only vary with the stability parameter ($s = f(\zeta)z$). This length scale should be a characteristic length scale of the large turbulent eddies given that the dissipation rate has already been assumed to be equal to the production rate of TKE (Eq. 12). Similar to Eq. 13, one can write

$$\begin{aligned} K_m &= A'' \left(u_*^2 \frac{dU}{dz} + \frac{g}{\Theta} \overline{w'\theta'} \right)^{1/3} z^{4/3} \left(\frac{s}{z} \right)^{4/3} \\ &= \frac{A''}{\kappa^{1/3}} u_* z (\phi_m - \zeta)^{1/3} \left(\frac{s}{z} \right)^{4/3}, \end{aligned} \quad (18)$$

where A'' is a proportionality coefficient. After imposing $\phi_m(0) = 1$, this leads to

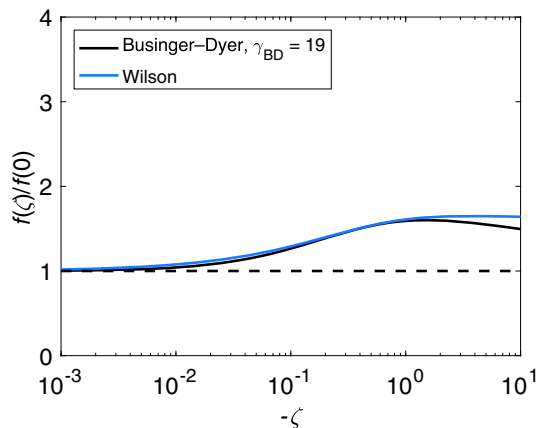
$$\phi_m^4 - \zeta \phi_m^3 = \frac{1}{[f(\zeta)/f(0)]^4}, \quad (19)$$

and $A'' = (\kappa/f(0))^{4/3}$, where $f(0)$ is the normalized length scale under neutral conditions. This will be called the extended O'KEYPS equation herein, which recovers the O'KEYPS equation with $\gamma_{\text{OKEYPS}} = 1$ if a constant f is used.

From a historical perspective, this was in fact one of the first derivations of the O'KEYPS equation by Kazansky and Monin (1956) and Kazansky and Monin (1958), but the challenge with it lies in the difficulty of quantifying $f(\zeta)/f(0)$, which is probably why it was not picked up by various researchers until much later.

New developments of phenomenological and cospectral budget models, which will be discussed in the following sections, are particularly helpful for understanding the role of s (or equivalently f). However, before introducing those models, it is enlightening to show the variation of $f(\zeta)/f(0)$ with $-\zeta$ required to reproduce the empirical functions (e.g., the Businger–Dyer relation or the Wilson formulation). To do so, the Businger–Dyer relation and the Wilson formulation are substituted into Eq. 19 to obtain $f(\zeta)/f(0)$, as shown in Fig. 3. It is clear that $f(\zeta)/f(0)$ increases with increasing $-\zeta$ and levels off towards a constant of about 1.6 for Wilson's formulation, a result due to the $-1/3$ scaling of ϕ_m in Wilson's formulation. The value of 1.6 is extremely close to the 1.7 value in Businger's model. The

Fig. 3 The variation of $f(\zeta)/f(0)$ computed using Eq. 19 with the Businger–Dyer relation ($\gamma_{BD} = 19$) and the Wilson formulation



agreement suggests that this extension of the O'KEYPS equation (i.e., introducing a stability-dependent length scale) leads to a similar finding as Businger's model. That is, the length scale that characterizes turbulent transport under convective conditions is about twice of its counterpart under neutral conditions. In fact, one can formally show that under convective conditions, substituting $\phi_m = a(-\zeta)^{-1/3}$ into the O'KEYPS equation (Eq. 5), Businger's model (Eq. 17), and the extended O'KEYPS equation (Eq. 19) yields

$$a^3 = \frac{1}{\gamma_{\text{OKEYPS}}} = \frac{1}{[s_c/s_m]^4} = \frac{1}{[f(-\infty)/f(0)]^4}. \quad (20)$$

This demonstrates that the coefficient in the fitted ϕ_m functions, the empirical coefficient in the O'KEYPS equation, and the ratio of length scales under convective and neutral conditions in both Businger's model and the extended O'KEYPS equation are closely linked.

4 Phenomenological Models

4.1 An Isotropic Eddy

Recently there has been renewed interest in understanding the behaviour of ϕ_m based on phenomenological considerations illustrated in Fig. 4 (Gioia et al. 2010; Katul et al. 2011; Salesky et al. 2013; Li et al. 2016b). Consistent with Monin–Obukhov similarity theory, the turbulent shear stress is assumed to be height-independent and thus equals to u_*^2 . At height z , the turbulent shear stress generated by an imaginary, isotropic turbulent eddy of size s (see Fig. 4a) can be expressed as

$$u_*^2 = -\overline{u'w'} \propto w_{\text{int}}(s)[U(s+z) - U(s-z)] \propto w_{\text{int}}(s) \frac{dU}{dz} 2s, \quad (21)$$

where $w_{\text{int}}(s)$ is the eddy turnover velocity, and $[U(s+z) - U(s-z)]$ denotes the mean velocity difference (i.e., net momentum per unit mass) across the eddy in the vertical direction.

The eddy turnover velocity is the key new quantity here, which may be estimated as $w_{\text{int}} = (\int_{1/s}^{\infty} E_w(k) dk)^{1/2}$ where $E_w(k)$ is the vertical velocity energy spectrum and k is the scalar wavenumber. Note that Gioia et al. (2010) used the TKE spectrum, but the use of the vertical velocity energy spectrum seems to be more appropriate (Katul and Manes

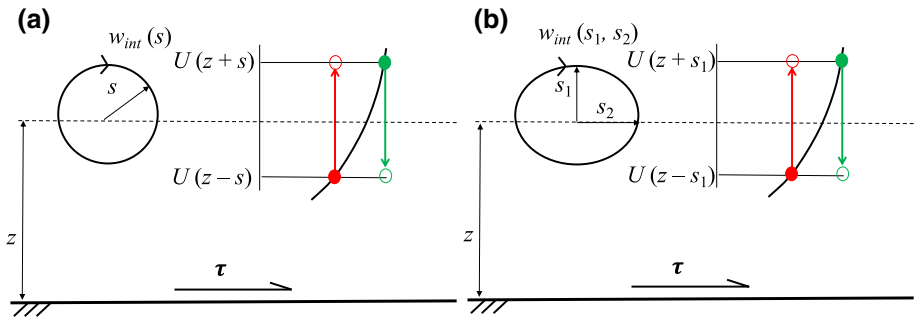


Fig. 4 A schematic of momentum transport by a single turbulent eddy (not to scale). **a** depicts an isotropic eddy and **b** depicts an anisotropic eddy

2014). If the vertical velocity energy spectrum is assumed to follow the Kolmogorov $-5/3$ law from $k = 1/s$ to $k = \infty$, then $w_{\text{int}} = (\int_{1/s}^{\infty} E_w(k) dk)^{1/2}$ yields $w_{\text{int}} \propto (\epsilon s)^{1/3}$. It is immediately clear that Eq. 21 corresponds to an eddy viscosity $K_m \propto (\epsilon s)^{1/3} s$, Heisenberg's eddy viscosity.

The phenomenological model further assumes that the dissipation rate of TKE is in equilibrium with the production rate of TKE (Eq. 12), and the size of the dominant turbulent eddies in the atmospheric surface layer scales with the height above the ground z , namely, $s = f(\zeta)z$, where $f(\zeta)$ represents the impact of atmospheric instability on the size of the dominant turbulent eddies. These are the same assumptions invoked in the derivation of the extended O'KEYPS equation. As a result, the phenomenological model recovers Eq. 19.

4.2 Eddy Anisotropy

Instead of an isotropic eddy, Salesky et al. (2013) assumed an anisotropic eddy characterized by s_1 and s_2 (see Fig. 4b), where $s_1 = f_1(\zeta)z$ and $s_2 = f_2(\zeta)z$. To estimate the eddy turnover velocity, the one-dimensional spectrum in the streamwise direction, which is typically reported in atmospheric surface-layer experiments (Kaimal and Finnigan 1994), is used. This yields $w_{\text{int}} = (\int_{1/s_2}^{\infty} E_w(k_x) dk_x)^{1/2}$, where k_x is the wavenumber in the streamwise direction. With this important modification, Eq. 19 becomes

$$\phi_m^4 - \zeta \phi_m^3 = \frac{1}{[f_1(\zeta)/f_1(0)]^3 [f_2(\zeta)/f_2(0)]}. \quad (22)$$

Although the effects of atmospheric instability on s_1 and s_2 are likely related (as will be seen later), introducing eddy anisotropy has the benefit of quantifying the impact of changing length scale in the vertical direction on ϕ_m separately from the impact of changing velocity scale. The former is reflected in $f_1(\zeta)/f_1(0)$, while the latter is reflected in $f_2(\zeta)/f_2(0)$ (see Fig. 4b). From Eq. 22 one can see that if f_1 is not too far away from f_2 , f_1 affects ϕ_m more significantly than f_2 . This is primarily because the eddy turnover velocity is proportional to the horizontal length of the eddy to the power of $1/3$ ($w_{\text{int}} \propto (\epsilon s_2)^{1/3}$).

Two points need to be clarified here. First, the two-dimensional anisotropic eddy shown in Fig. 4b remains an idealization. It should not be directly compared to the large-scale motions such as roll and cellular structures mentioned earlier. Second, although Eq. 22 recovers Eq. 19 when $f_2(\zeta)/f_2(0) = f_1(\zeta)/f_1(0)$, $f_2(\zeta)/f_2(0) = f_1(\zeta)/f_1(0)$ is not equivalent to assuming an isotropic eddy since $f_2(0)$ might be different from $f_1(0)$. In fact,

$f_2(\zeta)/f_2(0) = f_1(\zeta)/f_1(0)$ is a less stringent condition than assuming an isotropic eddy as it only means that the horizontal and vertical length scales are affected by instability similarly.

5 The Cospectral Budget Model

Another recently developed approach is based on the cospectral budget for momentum flux (Katul et al. 2013b). In the idealized atmospheric surface layer, turbulent momentum flux is primarily generated by shear production and destroyed by pressure–velocity decorrelation (Stull 1988). A similar equilibrium for the momentum flux budget in the spectral space, specifically in the inertial subrange, is assumed

$$0 = P(k) + \pi(k) = -\frac{2}{3}E(k)\frac{dU}{dz} + \pi(k), \quad (23)$$

where $P(k)$ is the production rate of momentum flux at wavenumber k and $\pi(k)$ is the pressure–velocity decorrelation term at k for which the following parametrization is invoked

$$\pi(k) = -c_\tau \frac{F_{uw}(k)}{\epsilon^{-1/3}k^{-2/3}}, \quad (24)$$

where c_τ is a coefficient. More complicated parametrizations for $\pi(k)$ have been used (Katul and Manes 2014; Katul et al. 2013a, 2014; Li and Katul 2017), but they do not change the main result. With these two equations and $E(k) = c_o \epsilon^{2/3}k^{-5/3}$, where c_o is again the Kolmogorov constant, one arrives at

$$F_{uw}(k) = -\left(\frac{2c_o}{3c_\tau}\right)\epsilon^{1/3}k^{-7/3}\frac{dU}{dz}. \quad (25)$$

The total momentum flux is $\int_0^\infty F_{uw}(k)dk$, which is further assumed to be proportional to the integrated momentum flux between $k = 1/s$ and $k = \infty$. Hence, $-u_*^2 = c_1 \int_{1/s}^\infty F_{uw}(k)dk$, where c_1 is a proportionality coefficient. A more physically based calculation of c_1 is provided by assuming a constant energy spectrum in the range of $k = 0$ and $k = 1/s$ (Katul et al. 2013b). With Eq. 25, $u_*^2 = \left(\frac{c_1 c_o}{2c_\tau}\right)\epsilon^{1/3}s^{4/3}(dU/dz)$, which recovers an eddy viscosity of $K_m \propto \epsilon^{1/3}s^{4/3} \propto (\epsilon s)^{1/3}s$. Similar to previous derivations, assuming $s = f(\zeta)z$ and imposing $\phi_m(0) = 1$ yields Eq. 19.

One can compare the cospectral budget model to Businger's model. In the cospectral budget model (and also in the phenomenological model), the inertial subrange starts from $k = 1/s = 1/(f(\zeta)z)$ (see Fig. 2b). As instability increases, the cospectral budget and phenomenological models implicitly assume that the inertial subrange extends gradually to lower wavenumber (i.e., with increasing f). However, in Businger's model, the inertial subrange is fixed in terms of its extent but is split into two parts. The first part extends from k_c to k_m and the second part starts from k_m , and these two parts have different dissipation rates. Consequently, the instability effect in Businger's model is reflected by the relative increase of the dissipation rate in the first part of the inertial subrange as $-\zeta$ increases (see Fig. 2a).

6 The Change of Length Scale with Instability

It is clear that the O'KEYPS equation when derived based on the dissipation rate of TKE, and recent developments such as the phenomenological model and the cospectral budget model

have the same physical basis, which is Heisenberg's eddy viscosity: $K_m \propto \epsilon^{1/3} s^{4/3}$. All these different derivations converge because the eddy viscosity is constrained by dimensional homogeneity, namely, it has to be a velocity scale, $(\epsilon s)^{1/3}$, multiplied by a length scale, s . However, only considering the buoyancy effect on the dissipation rate of TKE does not capture the observed ϕ_m under unstable conditions, as this leads to the O'KEYPS equation with $\gamma_{\text{O'KEYPS}} = 1$. To alleviate this problem, earlier studies focus on adjusting the velocity scale with empirical coefficients (Yamamoto 1959; Panofsky 1961). Note that introducing an empirical coefficient in the budget equation for TKE only affects the dissipation rate and hence only the velocity scale. On the other hand, later extensions of the O'KEYPS equations (including Businger's model that results in a slightly different final equation form), the phenomenological model, and the cospectral budget model focus on taking into account the impact of atmospheric instability on the length scale of dominant turbulent eddies.

Before presenting experimental data on the length scale, the two mixing lengths due to Prandtl and von Kármán are examined. One can see from Eq. 19 that it would be mathematically convenient if f could be linked back to ϕ_m , which would then allow Eq. 19 to be solved iteratively. The first possibility is to use Prandtl's mixing-length concept, $s = u_*/(dU/dz)$. In the neutral limit, this gives $f(0) = \kappa$. As such, $f(\zeta)/f(0) = 1/\phi_m$. However, substituting $f(\zeta)/f(0) = 1/\phi_m$ into Eq. 19 leads to a trivial and unphysical solution, $\phi_m = 0$ for any ζ . The second possibility is to employ von Kármán's mixing length, $s = -\kappa(dU/dz)/(d^2U/dz^2)$, which also gives $f(0) = \kappa$. Using the definition of ϕ_m , or $dU/dz = (\phi_m u_*)/(\kappa z)$, one can show that

$$\frac{f(\zeta)}{f(0)} = \frac{-\kappa \frac{\phi_m u_*}{\kappa z}}{\kappa z \frac{d\left(\frac{\phi_m u_*}{\kappa z}\right)}{dz}} = -\frac{\frac{\phi_m}{z}}{z \frac{d\left(\frac{\phi_m}{z}\right)}{dz}} = \frac{1}{1 - \frac{-\zeta}{\phi_m} \frac{d\phi_m}{d(-\zeta)}}. \quad (26)$$

Substituting Eq. 26 into Eq. 19 yields an increasing ϕ_m with increasing $-\zeta$, contrary to observations. Fundamentally, this is because von Kármán's mixing length decreases with increasing $-\zeta$, a well-known result since the 1950s (Deacon 1949; Businger 1959; Brutsaert and Yeh 1970); while to reproduce the observed behaviour of ϕ_m under unstable conditions, $f(\zeta)/f(0)$ needs to increase with increasing $-\zeta$ (see Fig. 3). The derivation of $f(\zeta)/f(0)$ presented here with the von Kármán mixing length is different from the derivation in Herbet and Panhans (1979), but the conclusion is the same. That is, using the mixing length of von Kármán does not produce the desired result for ϕ_m .

Physically, the failure of the two mixing lengths is understandable, as they are properties of the mean flow. The length scale s should reflect 'turbulence' properties (Pasquill 1972), especially those of large turbulent eddies that dominate momentum transfer. The logical follow-up option is the integral length scale of the vertical velocity. The integral length scale characterizes the scale over which the flow field remains correlated, which has been often interpreted as the size of the dominant turbulent eddies (Kaimal and Finnigan 1994) consistent with the phenomenological model (see Fig. 4). From the spectral perspective (see Fig. 2), the integral length scale roughly corresponds to the peak for $kE(k)$, which often marks the transition from the energy production range to the inertial subrange (Kaimal and Finnigan 1994). Thus one might argue that at this transition the inertial subrange scaling underlying Heisenberg's eddy viscosity still applies.

6.1 Data

The integral length scales of the vertical velocity can be calculated based on the autocorrelation ρ_{ww}

$$\rho_{ww}(\Delta x, \Delta z) = \frac{w'(x, y, z)w'(x + \Delta x, y, z + \Delta z)}{\sigma_w(x, y, z)\sigma_w(x + \Delta x, y, z + \Delta z)}, \quad (27)$$

where Δx and Δz are translation distances in the streamwise and vertical directions, respectively; w' is the vertical velocity fluctuation and σ_w is the standard deviation of w' . When eddy anisotropy is considered (Eq. 22), the integral length scales in both streamwise and vertical directions (s_1 and s_2) are needed, which can be computed by fitting an exponential function to the autocorrelation, as follows

$$\rho_{ww}(0, \Delta z) = e^{-\frac{|\Delta z|}{s_2}}, \quad (28)$$

$$\rho_{ww}(\Delta x, 0) = e^{-\frac{|\Delta x|}{s_1}}. \quad (29)$$

In field experiments, Taylor's frozen hypothesis is often invoked to compute $\Delta x = U \Delta t$, where U is the mean horizontal velocity and Δt is the translation distance in time. For multi-level eddy-covariance measurements, Δz is the distance between the measurement heights and the reference height.

Here the integral length scales of the vertical velocity are computed using two multi-level eddy-covariance datasets, one collected over a lake surface and the other collected over a dryland shrub surface. The two datasets have been used in multiple previous studies (Li and Bou-Zeid 2011; Li et al. 2012a, 2015a, 2016a; Finn et al. 2016a,b; Lan et al. 2018, 2019) and thus only the key experimental details are summarized here. The lake dataset has measurements at 1.65, 2.30, 2.95, and 3.65 m (Bou-Zeid et al. 2008; Vercauteren et al. 2008). The dryland dataset has measurements at 2, 8, 16, and 60 m (Finn et al. 2016a,b). For each 30-min data segment, linear detrending and double rotation are applied to the measured time series. The density correction (Webb et al. 1980) is applied to the computed latent heat flux (LE) and CO_2 flux but these fluxes are not used in this study. Data segments that satisfy the following conditions are excluded: (1) the mean flow originates from the back of the tower, (2) sensible heat flux (H) or u_* are too small ($H < 5 \text{ W m}^{-2}$ or $u_* < 0.05 \text{ m s}^{-1}$), (3) the stability parameter is positive, and (4) turbulent intensities are higher than 0.35.

Since both datasets used in this study only have four levels of eddy-covariance measurements, it is important to examine whether the vertical integral length scale can be computed with only four data points. Figure 5 shows two examples of computing the vertical integral length scale in the two datasets. The lowest measurement height is used as the reference level and thus Δz is simply the height difference between the remaining three levels and the lowest level. One can see that for the lake dataset, the four data points seem to constrain the data fitting reasonably well. For the dryland dataset, the four levels are much further apart, especially between the top most level (which is at 60 m) and the reference level.

Despite this concern for the dryland dataset, the vertical integral length scales are computed as shown in Fig. 6. The vertical integral length scales increase in the range of $0.01 < -\zeta < 1$ and approach a constant of about 2 at $-\zeta \approx 1$. Note that here $-\zeta$ is the stability parameter at the reference level (i.e., 1.65 m and 2 m for the lake and dryland datasets, respectively) and hence there are few data points for $-\zeta > 1$, although the computation of the vertical length scale requires data from all four levels. The computed vertical integral length scales from the lake and dryland datasets seem to follow an empirical function provided by Salesky et al. (2013), which was derived using data from the Advection Horizontal Array Turbulence

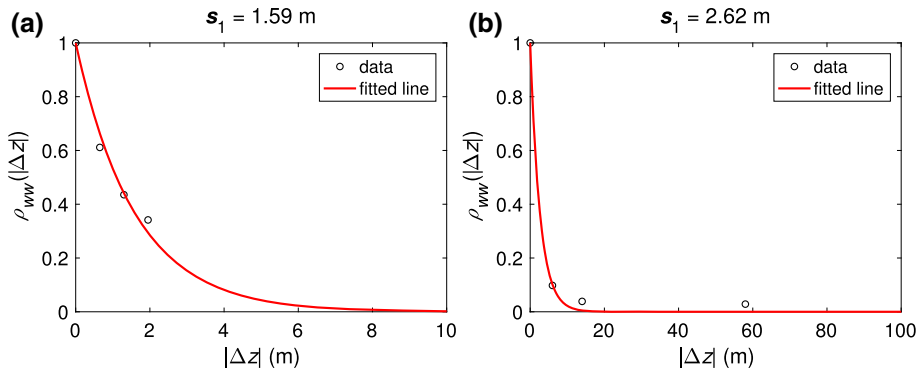


Fig. 5 **a** An example of computing the vertical integral length scale in the lake dataset. This particular example has $-\zeta = 0.01$ at 1.65 m. **b** An example of computing the vertical integral length scale in the dryland dataset. This particular example has $-\zeta = 0.01$ at 2 m

Study or AHATS (Salesky et al. 2012; Salesky and Chamecki 2012)

$$\left(\frac{f_1(\zeta)}{f_1(0)} \right)_{AHATS} = [1 - 0.514 (1 - e^{4.49\zeta})]^{-1}. \quad (30)$$

The dryland dataset shows more scatter because the measurement levels are further apart. However, the dryland dataset still follows the empirical function fairly well. The goodness-of-fit statistics indicate that the fitting procedure is acceptable for both datasets. For all fits in both datasets, the R^2 values are all larger than 0.95 and the root-mean-square errors are smaller than 0.08. The agreement between the lake and dryland datasets and the agreement with the empirical function derived from the AHATS experiment give further confidence in the computed vertical integral length scales.

The streamwise integral length scales computed using Taylor's frozen turbulence hypothesis are shown in Fig. 7. Here all four levels are shown for intercomparison and the thick line is the empirical function provided by Salesky et al. (2013), which was again derived from the AHATS experiment

$$\left(\frac{f_2(\zeta)}{f_2(0)} \right)_{AHATS} = [1 - 0.462 (1 - e^{4.82\zeta})]^{-1}. \quad (31)$$

Similar to the vertical integral length scale, the streamwise integral length scale increases in the range of $0.01 < -\zeta < 1$ and approaches a constant of about 2 at $-\zeta \approx 1$, and the computed scales agree with the empirical function. Here it should be noted that data from the Kansas experiment showed that the peak locations in the one-dimensional vertical velocity spectra, when normalized by the neutral value, also approach a constant when $-\zeta \approx 1$ (Kaimal and Finnigan 1994; Katul et al. 2011). Compared to the vertical integral length scale, more scatter is observed for the streamwise integral length scale, especially under moderately to strongly unstable conditions, which might be caused by the breakdown of Taylor's hypothesis when the mean flow becomes weak and when the turbulence intensity is high (Stull 1988). The scatter also could be related to the influence of the boundary-layer height as free convection is approached (Deardorff 1970; Panofsky et al. 1977; Hicks 1985; Johansson et al. 2001; McNaughton et al. 2007; Laubach and McNaughton 2009; Banerjee and Katul 2013), especially for the high levels.

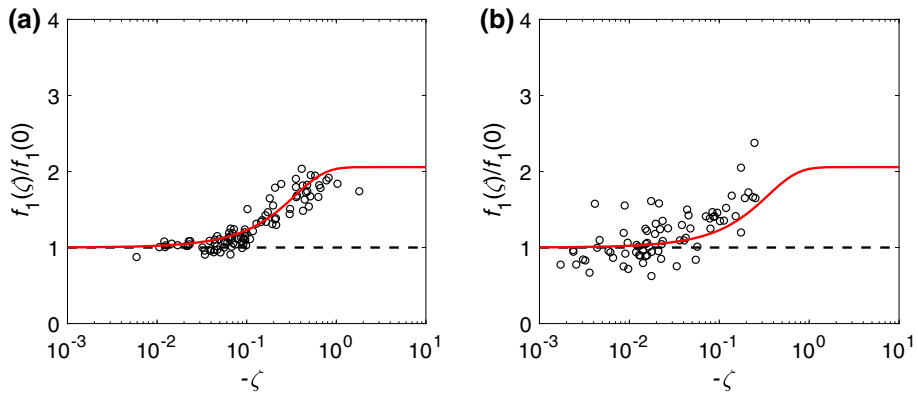


Fig. 6 The vertical integral length scale, normalized by its neutral value, as a function of $-\zeta$ in the **a** lake and **b** dryland datasets. Here $-\zeta$ is computed at 1.65 m and 2 m for the lake and dryland datasets, respectively. The thick line is the empirical function derived from the AHATS experiment and the dashed line indicates a constant of unity

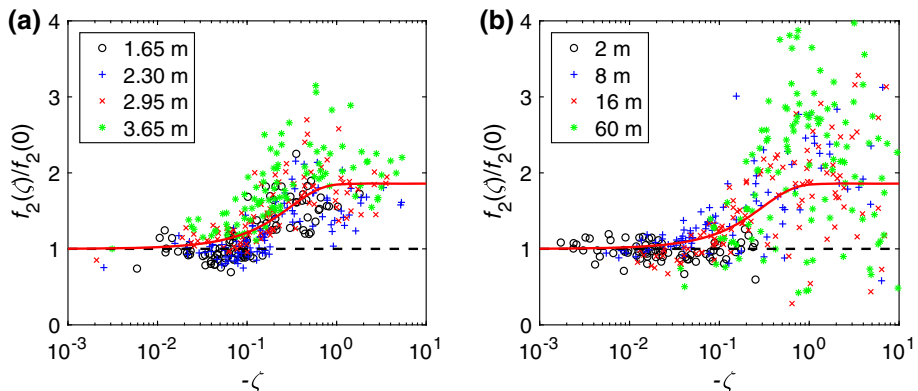


Fig. 7 The streamwise integral length scale, normalized by its neutral value, as a function of $-\zeta$ in the **a** lake and **b** dryland datasets. Here $-\zeta$ is computed at each height. The thick line is the empirical function derived from the AHATS experiment and the dashed line indicates a constant of unity

Figure 8 further shows the ratio of normalized streamwise to vertical integral length scales. This can be only done for the reference level, which is the lowest measurement height. As can be seen, only in the lake data are the two length scales affected by instability in a similar way (i.e., the ratios are close to unity). Close inspection of Fig. 7b reveals that the streamwise integral length scale at 2 m in the dryland dataset does not increase with instability, while the vertical integral length scale increases moderately with instability (see Fig. 6b). The effect of the dissimilar behaviours of $f_1(\zeta)/f_1(0)$ and $f_2(\zeta)/f_2(0)$ in the dryland dataset will be examined in the following subsection.

6.2 Connecting Data with Models

As discussed earlier, $f_1(\zeta)/f_1(0)$ and $f_2(\zeta)/f_2(0)$ are affected by atmospheric instability similarly in the lake dataset while dissimilarly in the dryland dataset. A natural follow-up

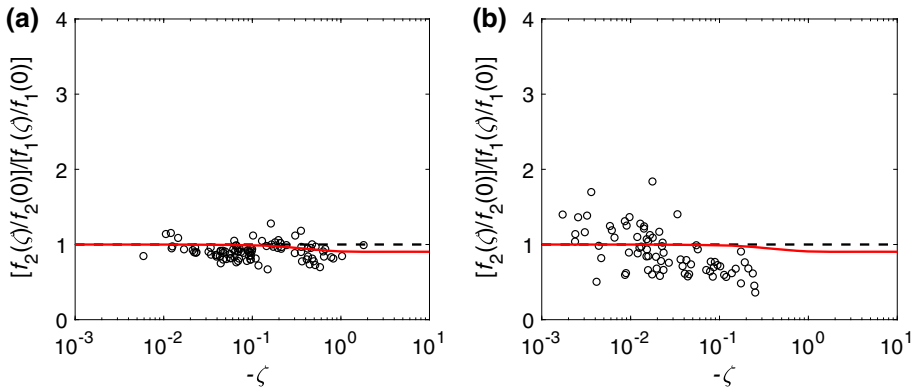


Fig. 8 The ratio of normalized streamwise to vertical integral length scales as a function of $-\zeta$ in the **a** lake and **b** dryland datasets. Here $-\zeta$ is computed at 1.65 m and 2 m for the lake and dryland datasets, respectively. The thick line is the empirical function derived from the AHATS experiment and the dashed line indicates a constant of unity

question is then how important is the dissimilarity between $f_1(\zeta)/f_1(0)$ and $f_2(\zeta)/f_2(0)$ in affecting the ϕ_m . To answer this question, the ϕ_m values computed using Eq. 22 with different scenarios are examined. These sensitivity tests allow the effects of atmospheric instability on the velocity and length scales forming the eddy viscosity to be quantified separately and jointly.

The first two scenarios are motivated by the lake data. In the first scenario (the orange dashed line in Fig. 9), it is assumed that $f_2(\zeta)/f_2(0) = f_1(\zeta)/f_1(0) = [f_1(\zeta)/f_1(0)]_{AHATS}$ (Eq. 30). In the second scenario (the red dashed line in Fig. 9), $f_1(\zeta)/f_1(0)$ and $f_2(\zeta)/f_2(0)$ are different and taken from the AHATS experiment (Eqs. 30 and 31). As can be seen, the two resulting ϕ_m are fairly close to each other, implying that the impact of atmospheric instability on eddy anisotropy is actually not very important in altering the behaviour of ϕ_m . Again, this does not mean that eddy anisotropy does not exist because the two functions, $f_2(\zeta)/f_2(0)$ and $f_1(\zeta)/f_1(0)$, have already removed the eddy anisotropy that might exist under neutral conditions [i.e., $f_2(0)$ might be different from $f_1(0)$]. The ratio of $f_1(0)/f_2(0)$ is 0.92 and 0.82 for the lake and dryland datasets, respectively. Specifically, $f_1(0) = 1.48$ m and $f_2(0) = 1.61$ m in the lake dataset and $f_1(0) = 1.69$ m and $f_2(0) = 2.05$ m in the dryland dataset. The difference in $f_1(0)/f_2(0)$ observed in these datasets might be related to the underlying surface conditions and also the definition of ‘neutral’. It was also shown that this ratio depends on how exactly f_1 is computed (Salesky et al. 2013). Nonetheless, the exact value of $f_1(0)/f_2(0)$ does not affect our finding. The fact that the first scenario yields a similar ϕ_m to the second scenario means that atmospheric instability does not introduce any additional anisotropic impacts, compared to the neutral conditions, that need to be considered from the perspective of capturing the variation of ϕ_m .

In the third scenario (the red line in Fig. 9), $f_2(\zeta)/f_2(0)$ is simply set to unity motivated by the dryland data. One can see that this produces ϕ_m values that are surprisingly in better agreement with the Kansas data and the other empirical functions. Recall that the impact of atmospheric instability on the velocity scale is reflected in $f_2(\zeta)/f_2(0)$ and the impact of atmospheric instability on the vertical length scale is reflected in $f_1(\zeta)/f_1(0)$. The results here imply that the impact of atmospheric instability on the velocity scale is actually not important for reproducing the behaviour of ϕ_m . This further suggests that trying to manipulate

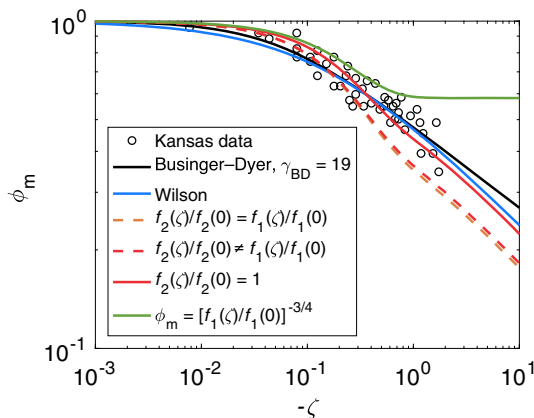


Fig. 9 The stability correction function ϕ_m . The circles represent data from the Kansas experiment. The black line is the Businger–Dyer relation with $\gamma_{BD} = 19$. The blue line is the Wilson formulation. The orange and red dashed lines are the solutions of the phenomenological model (Eq. 22) with $f_2(\zeta)/f_2(0) = f_1(\zeta)/f_1(0)$ and $f_2(\zeta)/f_2(0) \neq f_1(\zeta)/f_1(0)$. The red line is the solution of the phenomenological model (Eq. 22) with $f_2(\zeta)/f_2(0) = 1$. The green line is the result when the atmospheric instability effect on the velocity scale is completely ignored

the velocity scale by introducing an empirical coefficient in earlier derivations of O'KEYPS equation (Yamamoto 1959; Panofsky 1961) is physically ungrounded.

It should be stressed that this does not mean that the impact of atmospheric instability on the velocity scale is completely ignored because the impact of atmospheric instability on the dissipation rate of TKE is still considered. If the buoyancy effect on the dissipation rate of TKE was further neglected, the result would be $\phi_m = [f_1(\zeta)/f_1(0)]^{-3/4}$. As shown in Fig. 9, this causes the ϕ_m to deviate from observations for $-\zeta > 1$ and effectively destroys the $-1/3$ scaling of ϕ_m in the convective limit. This, together with the fact that the vertical length scale approaches a constant around $-\zeta \approx 1$, implies that when $-\zeta$ becomes large than 1, the impact of atmospheric instability on ϕ_m is mostly through the velocity scale and can be adequately captured by the dissipation rate of TKE under local equilibrium. However, in the widely observed unstable regime ($0.01 < -\zeta < 1$), the increase of vertical length scale is the most important factor responsible for the decrease of ϕ_m .

Overall, these sensitivity tests suggest that the observed reduction of ϕ_m when $-\zeta < 1$ is strongly related to the increasing length scale of dominant turbulent eddies in the vertical direction. This seems to be reasonable given that turbulent transport considered here is essentially a vertical problem. This further implies that introducing an empirical coefficient in the velocity scale, as typically done in earlier derivations of the O'KEYPS equation, is ungrounded. It is only when $-\zeta > 1$ that the impact of atmospheric instability on the velocity scale becomes important, which can be adequately captured by considering the buoyancy effects on the dissipation (or production) rate of TKE.

7 Revisiting the Assumption of a Constant Turbulent Prandtl Number

Now let us return to the first derivation, in which a constant turbulent Prandtl number is assumed. Under such assumption, $\gamma_{O'KEYPS} = (Pr_t c^{\text{con}})^3 / \kappa^4$ (Eq. 11). This, combined with

the convective limit result (Eq. 20), gives

$$\frac{f(-\infty)}{f(0)} = (\gamma_{\text{OKEYPS}})^{1/4} = \frac{(Pr_t c^{\text{con}})^{3/4}}{\kappa} \propto \frac{1}{\kappa}. \quad (32)$$

This simple result shows the merit of the interpolation formulation used by Ellison (1957) and Sellers (1962), despite its assumption of a constant turbulent Prandtl number: it has implicitly used a length scale of κz under neutral conditions and of $\sim z$ (see Eq. 6) under convective conditions. That is, it has implicitly considered an increase in the length scale by a factor of $1/\kappa = 2.5$. In contrast, earlier derivations of the O'KEYPS equation based on the dissipation rate of TKE (Yamamoto 1959; Panofsky 1961) implicitly used κz as the length scale for all unstable conditions (see Eqs. 13 and 14). This demonstrates, from another perspective, why earlier derivations of the O'KEYPS equation based on the dissipation rate of TKE (Yamamoto 1959; Panofsky 1961) had to always introduce an empirical coefficient in their velocity scale in order to compensate their neglect of changes in the length scale. This also explains why Obukhov (1971) and Fleagle and Businger (1981) had to introduce an empirical coefficient in their heuristic arguments supporting the interpolation formulation used by Ellison (1957) and Sellers (1962) because they focused solely on the velocity scale too (note that these arguments are not presented here).

The finding that the ratio of the convective and neutral length scales is approximately $1/\kappa = 2.5$ was actually conjectured by Kazansky and Monin (1956, 1958) (see the nice illustration in Naito 1964). From Eq. 32 one can see that the turbulent Prandtl number, which is generally smaller than unity under unstable conditions, acts to reduce this ratio from $1/\kappa = 2.5$. Recall that the observational data in the previous section show that the ratio of the convective and neutral length scales is about 2 (Fig. 6) and a value of 1.6 is needed to reproduce Wilson's formulation (Fig. 3).

A variable Pr_t can be introduced to examine how the variation of Pr_t alters the ϕ_m resulting from the O'KEYPS equation. To do so a model for Pr_t is needed. One possible candidate is the Pr_t formulation from the cospectral budget model (Katul et al. 2014; Li et al. 2015b; Li 2016, 2019)

$$Pr_t = Pr_t^{\text{neu}} \left(1 + \omega \frac{-\zeta}{\phi_m - \zeta} \right)^{-1}, \quad (33)$$

where ω is a coefficient. In a landmark study by Katul et al. (2014), it was shown that ω only depends on the ratio of the one-dimensional Obukhov–Corrsin constant for temperature spectrum to the one-dimensional Kolmogorov constant for vertical velocity spectrum, and an isotropization constant in the Rotta model for pressure-scalar decorrelation (Pope 2000). Later studies indicate that ω can be also modulated by the shape of turbulence energy spectra, which is particularly important under unstable conditions (Li et al. 2015b; Li 2016, 2019). Hence ω is treated as a coefficient here. One nice property of this model is that it approaches a non-zero value in the convective limit, namely $Pr_t^{\text{con}} = Pr_t^{\text{neu}}(1 + \omega)^{-1}$, thus ensuring the recovery of the $-1/3$ scaling for ϕ_m . Note that empirically fitted models for Pr_t often give $Pr_t^{\text{con}} = 0$ (see e.g., Pandolfo 1966, and Maronga and Reuder 2017), which would not recover the $-1/3$ scaling for ϕ_m . Substituting Eq. 33 into Eq. 10 yields

$$\phi_m^4 - \frac{(Pr_t^{\text{neu}} c^{\text{con}})^3}{(1 + \omega)^2 \kappa^4} \left(1 + \omega \frac{-\zeta}{\phi_m - \zeta} \right)^{-1} \phi_m^3 \zeta = 1. \quad (34)$$

The above two equations have three coefficients (Pr_t^{neu} , c^{con} , ω) that need to be determined, and thus some tuning is required. With $Pr_t^{\text{neu}} = 1$, $c^{\text{con}} = 1.7$, $\omega = 2$, the resulting

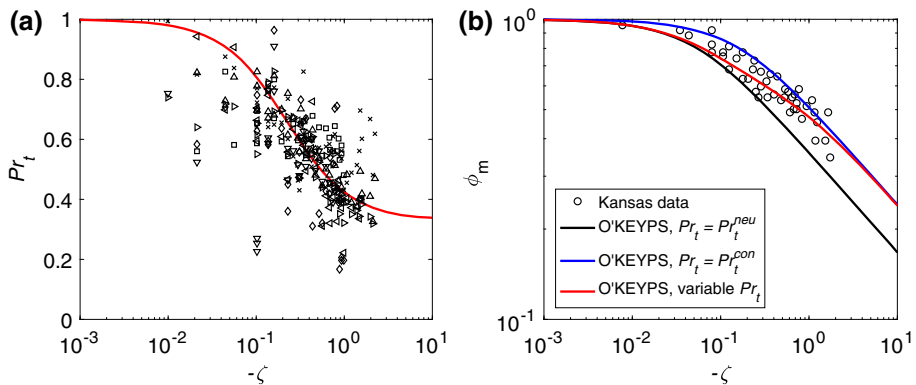


Fig. 10 **a** The Pr_t as a function of $-\zeta$. The red line is from the cospectral budget model (Eq. 33). The markers indicate various experimental datasets collected by Li et al. (2015b). **b** The stability correction function ϕ_m . The circles are data from the Kansas experiment. The red line is the solution of Eq. 34. The black and blue lines are solutions of Eq. 10 with constant values of Pr_t , which are equal to the neutral and convective limits from Eq. 33, respectively

Pr_t and ϕ_m are shown in Fig. 10. One can see that the resulting Pr_t agrees with the experimental data fairly well (see Fig. 10a), suggesting that the values of these coefficients are not unreasonable. And the exact values of these coefficients are not the key point here. The key point is how the variation of Pr_t changes the predicted behaviour of ϕ_m . To make this clear, the ϕ_m from the O'KEYPS equation with a constant Pr_t (equal to its neutral or convective limit) is also shown (see Fig. 10b). One can see that under near-neutral conditions, the ϕ_m from variable Pr_t is closer to that from $Pr_t = Pr_t^{neu}$. As instability increases, the ϕ_m from variable Pr_t gradually shifts to that from $Pr_t = Pr_t^{con}$. This result suggests that some of the scatter in ϕ_m in field experiments and simulations might be associated with the variability of Pr_t , which is usually large (see Fig. 10a).

8 Summary and Future Outlook

The key findings of this study are (1) Heisenberg's eddy viscosity and local equilibrium in the TKE budget equation provide a unifying framework for many semi-empirical theories in the literature that lead to the O'KEYPS equation and its extension, and (2) the length scale characterizing turbulent transport in the vertical direction is the most critical factor controlling the behaviour of ϕ_m in the widely observed unstable regime ($0.01 < -\zeta < 1$) and can be reasonably constrained by a few (in this study only four) vertical measurements. The importance of the vertical length scale is not too surprising given that turbulent transport is essentially a vertical problem in an idealized atmospheric surface layer. The importance of the vertical length scale is also consistent with a recent study that focused on stable conditions (Li et al. 2016b). Using the same phenomenological model described in this study, Li et al. (2016b) showed that the Ozmidov length scale becomes a stronger constraint on turbulent transport in the vertical direction as the stability parameter becomes larger than 0.2, which needs to be taken into account in order to reproduce the behaviour of ϕ_m under moderately stable conditions.

All results regarding the convective limit in this paper are simple extrapolations to $-\zeta \sim \infty$ (e.g., the O'KEYPS equation and the fitted equations for the length scales). In particular,

it is shown that the asymptotic behaviours of ϕ_m and $f(\zeta)/f(0)$ [i.e., the $-1/3$ scaling law for ϕ_m and a constant $f(\zeta)/f(0)$] are closely linked to the assumption of a non-zero turbulent Prandtl number in the convective limit, which relates the eddy viscosity to the eddy diffusivity for heat that is much better constrained (Prandtl 1932; Priestley 1954, 1955, 1957, 1959). However, free convection seldom occurs in the real atmosphere (e.g., in observations there are few cases with $-\zeta > 1$). Hence, the behaviour of ϕ_m when the free convection is approached, despite being of considerable interest, remains elusive. Kader and Yaglom (1990) used directional dimensional analysis to show that ϕ_m should scale with $(-\zeta)^{1/3}$ instead of $(-\zeta)^{-1/3}$. Another support for the $1/3$ scaling is the local-free-convection similarity theory. As discussed early, the velocity and length scales for local free convection are w_* and z . Hence similarity theory would yield a constant $z/w_*(dU/dz)$. This, combined with $w_*/u_* \propto (-\zeta)^{1/3}$, would further give $\phi_m \propto (-\zeta)^{1/3}$ (Businger 1973). Experimental data have shown that the local-free-convection similarity theory describes the vertical velocity and temperature variances reasonably well (Kaimal and Finnigan 1994; Wyngaard 2010), but the prediction of the $1/3$ scaling for ϕ_m remains debated. Moreover, the $1/3$ scaling for ϕ_m , as well as the $1/3$ scaling for the vertical velocity variance, suggested by the local-free-convection similarity theory may suffer from self-correlation when observational data are used to determine them (Hicks 1978, 1981; Andreas and Hicks 2002; Klipp and Mahrt 2004). Recent large-eddy simulations seem to show a $1/3$ scaling for ϕ_m at large $-\zeta$ (Maronga and Reuder 2017; Li et al. 2018b), but the results are far from conclusive. It should be also highlighted that the $1/3$ scaling of ϕ_m would imply a zero turbulent Prandtl number under the free convective limit.

As free convection is approached, cellular structures (e.g., thermals) scaling with the boundary-layer height become the dominant flow feature (Wyngaard 1985; Schmidt and Schumann 1989; Salesky et al. 2017). This might introduce dependences of atmospheric surface layer variables on the boundary-layer height, thereby invalidating Monin–Obukhov similarity theory (Deardorff 1970; Panofsky et al. 1977; Hicks 1985; Johansson et al. 2001; McNaughton et al. 2007; Laubach and McNaughton 2009; Banerjee and Katul 2013). Recent work has started to incorporate the boundary-layer height into phenomenological and spectral models (Banerjee et al. 2015; Li et al. 2015b; Banerjee et al. 2016; McColl et al. 2017). Nonetheless, validating the role of boundary-layer height in such models remains a grand challenge considering that the boundary-layer height is not often measured in field experiments and, even when measured, tends to have large uncertainties (Seidel et al. 2010; Dai et al. 2014; Zhang et al. 2014). Associated with the influence of the boundary-layer height is the breakdown of the local flux-gradient relation due to non-local transport (Ertel 1942; Priestley and Swinbank 1947; Holtslag and Moeng 1991; Holtslag and Boville 1993; Zilitinkevich et al. 1999; van Dop and Verver 2001; Li et al. 2012b, 2018a), which poses further challenges to determining the behaviour of ϕ_m as free convection is approached. Further investigations in this area are strongly needed.

Acknowledgements This material is based upon work supported by the U.S. National Science Foundation under Grant AGS-1853354. This paper was completed when I was visiting Leibniz University Hannover, while supported by the Alexander von Humboldt Foundation. I thank Professor Marc Parlange and Professor Heping Liu for allowing me to use the lake and dryland datasets.

References

- Ali SZ, Dey S (2018) Impact of phenomenological theory of turbulence on pragmatic approach to fluvial hydraulics. *Phys Fluids* 30(4):045,105

- Andreas E, Hicks BB (2002) Comments on “critical test of the validity of Monin–Obukhov similarity during convective conditions”. *J Atmos Sci* 59(17):2605–2607
- Banerjee T, Katul G (2013) Logarithmic scaling in the longitudinal velocity variance explained by a spectral budget. *Phys Fluids* 25(125):106
- Banerjee T, Katul G, Salesky S, Chamecki M (2015) Revisiting the formulations for the longitudinal velocity variance in the unstable atmospheric surface layer. *Q J R Meteorol Soc* 141(690):1699–1711
- Banerjee T, Li D, Juang JY, Katul G (2016) A spectral budget model for the longitudinal turbulent velocity in the stable atmospheric surface layer. *J Atmos Sci* 73(1):145–166
- Bou-Zeid E, Vercauteren N, Parlange M, Meneveau C (2008) Scale dependence of subgrid-scale model coefficients: an a priori study. *Phys Fluids* 20(11):115106
- Brutsaert W, Yeh GT (1970) A power wind law for turbulent transfer computations. *Water Resour Res* 6(5):1387–1391
- Businger J (1959) A generalization of the mixing-length concept. *J Meteorol* 16(5):516–523
- Businger J (1961) On the relation between the spectrum of turbulence and the diabatic wind profile. *J Geophys Res* 66(8):2405–2409
- Businger J (1973) A note on free convection. *Boundary-Layer Meteorol* 4(1–4):323–326
- Businger JA (1988) A note on the Businger–Dyer profiles. *Boundary-Layer Meteorol* 42:145–151
- Businger JA, Yaglom AM (1971) Introduction to Obukhov’s paper on ‘Turbulence in an atmosphere with a non-uniform temperature’. *Boundary-Layer Meteorol* 2:3–6
- Businger JA, Wyngaard JC, Izumi Y, Bradley EF (1971) Flux-profile relationships in the atmospheric surface layer. *J Atmos Sci* 28(2):181–191
- Carper MA, Porté-Agel F (2004) The role of coherent structures in subfilter-scale dissipation of turbulence measured in the atmospheric surface layer. *J Turbul* 5:32–32
- Chauhan K, Hutchins N, Monty J, Marusic I (2013) Structure inclination angles in the convective atmospheric surface layer. *Boundary-Layer Meteorol* 147:1–10
- Dai C, Wang Q, Kalogiros J, Lenschow D, Gao Z, Zhou M (2014) Determining boundary-layer height from aircraft measurements. *Boundary-Layer Meteorol* 152(3):277–302
- Deacon E (1949) Vertical diffusion in the lowest layers of the atmosphere. *Q J R Meteorol Soc* 75(323):89–103
- Deardorff JW (1970) Convective velocity and temperature scales for the unstable planetary boundary layer and for Rayleigh convection. *J Atmos Sci* 27(8):1211–1213
- Dop H, Verver G (2001) Countergradient transport revisited. *J Atmos Sci* 58(15):2240–2247
- Dyer A (1974) A review of flux-profile relationships. *Boundary-Layer Meteorol* 7(3):363–372
- Dyer A, Hicks B (1970) Flux-gradient relationships in the constant flux layer. *Q J R Meteorol Soc* 96(410):715–721
- Ellison T (1957) Turbulent transport of heat and momentum from an infinite rough plane. *J Fluid Mech* 2(5):456–466
- Ertel H (1942) Ein neuer hydrodynamischer wirbelsatz. *Meteorol Z* 59:277–281
- Etling D, Brown R (1993) Roll vortices in the planetary boundary layer: a review. *Boundary-Layer Meteorol* 65(3):215–248
- Finn D, Clawson KL, Eckman RM, Liu H, Russell ES, Gao Z, Brooks S (2016a) Project Sagebrush: revisiting the value of the horizontal plume spread parameter y . *J Appl Meteorol Clim* 55(6):1305–1322
- Finn D, Reese B, Butler B, Wagenbrenner N, Clawson K, Rich J, Russell E, Gao Z, Liu H (2016b) Evidence for gap flows in the Birch Creek Valley, Idaho. *J Atmos Sci* 73(12):4873–4894
- Fleagle RG, Businger JA (1981) An introduction to atmospheric physics. Academic Press, New York
- Garratt JR (1994) The atmospheric boundary layer. Cambridge University Press, UK
- Gioia G, Guttenberg N, Goldenfeld N, Chakraborty P (2010) Spectral theory of the turbulent mean-velocity profile. *Phys Rev Lett* 105:184501
- Heisenberg W (1948) Zur statistischen theorie der turbulenz. *Z Physik* 124(7):628–657
- Herbet F, Panhans WG (1979) Theoretical studies of the parameterization of the non-neutral surface boundary layer. *Boundary-Layer Meteorol* 16(2):155–167
- Hicks BB (1978) Some limitations of dimensional analysis and power laws. *Boundary-Layer Meteorol* 14(4):567–569
- Hicks BB (1981) An examination of turbulence statistics in the surface boundary layer. *Boundary-Layer Meteorol* 21(3):389–402
- Hicks BB (1985) Behavior of turbulence statistics in the convective boundary layer. *J Clim Appl Meteorol* 24(6):607–614
- Högström U (1988) Non-dimensional wind and temperature profiles in the atmospheric surface layer: a re-evaluation. *Boundary-Layer Meteorol* 1–2:55–78
- Högström U (1996) Review of some basic characteristics of the atmospheric surface layer. *Boundary-Layer Meteorol* 78(3–4):215–246

- Holtslag A, Boville B (1993) Local versus nonlocal boundary-layer diffusion in a global climate model. *J Clim* 6(10):1825–1842
- Holtslag A, Moeng CH (1991) Eddy diffusivity and countergradient transport in the convective atmospheric boundary layer. *J Atmos Sci* 48(14):1690–1698
- Hommema SE, Adrian RJ (2003) Packet structure of surface eddies in the atmospheric boundary layer. *Boundary-Layer Meteorol* 106(1):147–170
- Hutchins N, Chauhan K, Marusic I, Monty J, Klewicki J (2012) Towards reconciling the large-scale structure of turbulent boundary layers in the atmosphere and laboratory. *Boundary-Layer Meteorol* 145(2):273–306
- Johansson C, Smedman AS, Högström U, Brasseur JG, Khanna S (2001) Critical test of the validity of Monin–Obukhov similarity during convective conditions. *J Atmos Sci* 58(12):1549–1566
- Kader BA, Yaglom AM (1990) Mean fields and fluctuation moments in unstably stratified turbulent boundary-layers. *J Fluid Mech* 212:637–662
- Kaimal J, Finnigan J (1994) *Atmospheric boundary layer flows: their structure and measurement*. Oxford University Press, New York
- Katul G (2019) The anatomy of large-scale motion in atmospheric boundary layers. *J Fluid Mech* 858:1–4
- Katul G, Konings A, Porporato A (2011) Mean velocity profile in a sheared and thermally stratified atmospheric boundary layer. *Phys Rev Lett* 107:268502
- Katul G, Li D, Chamecki M, Bou-Zeid E (2013a) Mean scalar concentration profile in a sheared and thermally stratified atmospheric surface layer. *Phys Rev E* 87(2):023004
- Katul G, Porporato A, Manes C, Meneveau C (2013b) Co-spectrum and mean velocity in turbulent boundary layers. *Phys Fluids* 25(091):702
- Katul G, Porporato A, Shah S, Bou-Zeid E (2014) Two phenomenological constants explain similarity laws in stably stratified turbulence. *Phys Rev E* 89(1):023007
- Katul G, Li D, Manes C (2019) A primer on turbulence in hydrology and hydraulics: the power of dimensional analysis. *WIREs Water* 6(2):e1336
- Katul GG, Manes C (2014) Cospectral budget of turbulence explains the bulk properties of smooth pipe flow. *Phys Rev E* 90(063):008. <https://doi.org/10.1103/PhysRevE.90.063008>
- Kazansky A, Monin A (1956) Turbulence in the inversion layer near the surface. *Izv Akad Nauk SSSR Ser Geofiz* 1:79–86
- Kazansky A, Monin A (1958) On the turbulent regime in the near surface layer of air at unstable stratification. *Izv Akad Nauk SSSR Ser Geofiz* 6:741–751
- Khanna S, Brasseur JG (1997) Analysis of Monin–Obukhov similarity from large-eddy simulation. *J Fluid Mech* 345:251–286
- Klipp CL, Mahrt L (2004) Flux-gradient relationship, self-correlation and intermittency in the stable boundary layer. *Q J R Meteorol Soc* 130(601):2087–2103
- Kolmogorov A (1941) Dissipation of energy under locally isotropic turbulence. *Dokl Akad Nauk SSSR* 32:16–18
- Lan C, Liu H, Li D, Katul GG, Finn D (2018) Distinct turbulence structures in stably stratified boundary layers with weak and strong surface shear. *J Geophys Res Atmos* 123(15):7839–7854
- Lan C, Liu H, Katul GG, Li D, Finn D (2019) Large eddies regulate turbulent flux gradients in coupled stable boundary layers. *Geophys Res Lett* 46(11):6090–6100
- Laubach J, McNaughton KG (2009) Scaling properties of temperature spectra and heat-flux cospectra in the surface friction layer beneath an unstable outer layer. *Boundary-Layer Meteorol* 133(2):219–252
- Li D (2016) Revisiting the subgrid-scale Prandtl number for large-eddy simulation. *J Fluid Mech* 802:R2. <https://doi.org/10.1017/jfm.2016.472>
- Li D (2019) Turbulent Prandtl number in the atmospheric boundary layer: Where are we now? *Atmos Res* 216:86–105
- Li D, Bou-Zeid E (2011) Coherent structures and the dissimilarity of turbulent transport of momentum and scalars in the unstable atmospheric surface layer. *Boundary-Layer Meteorol* 140(2):243–262
- Li D, Katul GG (2017) On the linkage between the $k^{-5/3}$ spectral and $k^{-7/3}$ cospectral scaling in high-Reynolds number turbulent boundary layers. *Phys Fluids* 29(6):065,108
- Li D, Bou-Zeid E, de Bruin H (2012a) Monin–Obukhov similarity functions for the structure parameters of temperature and humidity. *Boundary-Layer Meteorol* 145(1):45–67
- Li D, Katul G, Bou-Zeid E (2012b) Mean velocity and temperature profiles in a sheared diabatic turbulent boundary layer. *Phys Fluids* 24(10):105105
- Li D, Katul G, Bou-Zeid E (2015a) Turbulent energy spectra and cospectra of momentum and heat fluxes in the stable atmospheric surface layer. *Boundary-Layer Meteorol* 157(1):1–21
- Li D, Katul GG, Zilitinkevich SS (2015b) Revisiting the turbulent Prandtl number in an idealized atmospheric surface layer. *J Atmos Sci* 72(6):2394–2410

- Li D, Katul G, Gentine P (2016a) The k^{-1} scaling of air temperature spectra in atmospheric surface layer flows. *Q J R Meteorol Soc* 142(694):496–505
- Li D, Salesky S, Banerjee T (2016b) Connections between the Ozmidov scale and mean velocity profile in stably stratified atmospheric surface layers. *J Fluid Mech* 797:R3. <https://doi.org/10.1017/jfm.2016.311>
- Li D, Katul GG, Liu H (2018a) Intrinsic constraints on asymmetric turbulent transport of scalars within the constant flux layer of the lower atmosphere. *Geophys Res Lett* 45(4):2022–2030
- Li Q, Gentine P, Mellado JP, McCol KA (2018b) Implications of nonlocal transport and conditionally averaged statistics on Monin–Obukhov similarity theory and Townsend’s attached eddy hypothesis. *J Atmos Sci* 75(10):3403–3431
- Liu HY, Bo TL, Liang YR (2017) The variation of large-scale structure inclination angles in high Reynolds number atmospheric surface layers. *Phys Fluids* 29(3):035,104
- Liu Y, Mamtimin A, Huo W, Yang X, Liu X, Yang F, He Q (2016) Nondimensional wind and temperature profiles in the atmospheric surface layer over the hinterland of the Taklimakan Desert in China. *Adv Meteorol*. <https://doi.org/10.1155/2016/9325953>
- Lumley JL, Panofsky HA (1964) The structure of atmospheric turbulence. Wiley, New York
- Maronga B, Reuder J (2017) On the formulation and universality of Monin–Obukhov similarity functions for mean gradients and standard deviations in the unstable surface layer: results from surface-layer-resolving large-eddy simulations. *J Atmos Sci* 74(4):989–1010
- McColl KA, van Heerwaarden CC, Katul GG, Gentine P, Entekhabi D (2017) Role of large eddies in the breakdown of the Reynolds analogy in an idealized mildly unstable atmospheric surface layer. *Q J R Meteorol Soc* 143(706):2182–2197
- McNaughton KG, Clement RJ, Moncrieff JB (2007) Scaling properties of velocity and temperature spectra above the surface friction layer in a convective atmospheric boundary layer. *Nonlinear Process Geophys* 14(3):257–271. <https://doi.org/10.5194/npg-14-257-2007>
- Monin A, Obukhov A (1954) Basic laws of turbulent mixing in the ground layer of the atmosphere. *Trudy Akad Nauk SSSR Geofiz Inst* 151:163–187
- Monin A, Yaglom A (1971) Statistical fluid mechanics, vol 1. MIT Press, Cambridge
- Naito K (1964) Some remarks on the Monin–Obukhov function in the atmosphere near the ground. *J Meteorol Soc Jpn Ser II* 42(1):53–64
- Obukhov A (1946) Turbulence in thermally inhomogeneous atmosphere. *Trudy Inta Teoret Geofiz Akad Nauk SSSR* 1:95–115
- Obukhov A (1971) Turbulence in an atmosphere with a non-uniform temperature. *Boundary-Layer Meteorol* 2(1):7–29
- Pandolfo JP (1966) Wind and temperature profiles for constant-flux boundary layers in lapse conditions with a variable eddy conductivity to eddy viscosity ratio. *J Atmos Sci* 23(5):495–502
- Panofsky H (1961) An alternative derivation of the diabatic wind profile. *Q J R Meteorol Soc* 87(371):109–110
- Panofsky H, Blackadar A, McVehil G (1960) The diabatic wind profile. *Q J R Meteorol Soc* 86(369):390–398
- Panofsky HA, Tennekes H, Lenschow DH, Wyngaard J (1977) The characteristics of turbulent velocity components in the surface layer under convective conditions. *Boundary-Layer Meteorol* 11(3):355–361
- Pasquill F (1972) Some aspects of boundary layer description. *Q J R Meteorol Soc* 98(417):469–494
- Patton EG, Sullivan PP, Shaw RH, Finnigan JJ, Weil JC (2016) Atmospheric stability influences on coupled boundary layer and canopy turbulence. *J Atmos Sci* 73(4):1621–1647
- Pirozzoli S, Bernardini M, Verzicco R, Orlandi P (2017) Mixed convection in turbulent channels with unstable stratification. *J Fluid Mech* 821:482–516
- Pope S (2000) Turbulent flows. Cambridge University Press, Cambridge
- Prandtl L (1932) Meteorologische anwendung der stromungslehre. *Beitr Phys Atmos* 19:188–202
- Priestley C (1954) Convection from a large horizontal surface. *Aust J Phys* 7(1):176–201
- Priestley C (1955) Free and forced convection in the atmosphere near the ground. *Q J R Meteorol Soc* 81(348):139–143
- Priestley C (1957) Convection from the earth’s surface. *Proc R Soc Lond Ser A* 238(1214):287–304
- Priestley C (1959) Turbulent transfer in the lower atmosphere. University of Chicago Press, Chicago
- Priestley C, Swinbank W (1947) Vertical transport of heat by turbulence in the atmosphere. *Proc R Soc Lond Ser A* 189(1019):543–561
- Salesky ST, Anderson W (2018) Buoyancy effects on large-scale motions in convective atmospheric boundary layers: implications for modulation of near-wall processes. *J Fluid Mech* 856:135–168
- Salesky ST, Anderson W (2020) Revisiting inclination of large-scale motions in unstably stratified channel flow. *J Fluid Mech* 884:R5. <https://doi.org/10.1017/jfm.2019.987>
- Salesky ST, Chamecki M (2012) Random errors in turbulence measurements in the atmospheric surface layer: implications for Monin–Obukhov similarity theory. *J Atmos Sci* 69(12):3700–3714

- Salesky ST, Chamecki M, Dias NL (2012) Estimating the random error in eddy-covariance based fluxes and other turbulence statistics: the filtering method. *Boundary-Layer Meteorol* 144(1):113–135
- Salesky ST, Katul GG, Chamecki M (2013) Buoyancy effects on the integral lengthscales and mean velocity profile in atmospheric surface layer flows. *Phys Fluids* 25(10):105101
- Salesky ST, Chamecki M, Bou-Zeid E (2017) On the nature of the transition between roll and cellular organization in the convective boundary layer. *Boundary-Layer Meteorol* 163(1):41–68
- Sander J (2000) On a general solution for eddy viscosity in the surface layer and implications to the diabatic wind profile. *Contrib Atmos Phys* 71(4)
- Schmidt H, Schumann U (1989) Coherent structure of the convective boundary layer derived from large-eddy simulations. *J Fluid Mech* 200:511–562
- Seidel DJ, Ao CO, Li K (2010) Estimating climatological planetary boundary layer heights from radiosonde observations: comparison of methods and uncertainty analysis. *J Geophys Res Atmos*. <https://doi.org/10.1029/2009JD013680>
- Sellers WD (1962) A simplified derivation of the diabatic wind profile. *J Atmos Sci* 19(2):180–181
- Shah S, Bou-Zeid E (2014) Very-large-scale motions in the atmospheric boundary layer deduced by snapshot proper orthogonal decomposition. *Boundary-Layer Meteorol* 153(3):355–387
- Song X, Zhang H, Chen J, Park SU (2010) Flux-gradient relationships in the atmospheric surface layer over the Gobi Desert in China. *Boundary-Layer Meteorol* 134(3):487–498
- Stull R (1988) An introduction to boundary layer meteorology. Kluwer Academic Publishers, Dordrecht
- Takeuchi K, Yokoyama O (1963) The scale of turbulence and the wind profile in the surface boundary layer. *J Meteorol Soc Jpn Ser II* 41(2):108–117
- Vercauteren N, Bou-Zeid E, Parlange MB, Lemmin U, Huwald H, Selker J, Meneveau C (2008) Subgrid-scale dynamics for water vapor, heat, and momentum over a lake. *Boundary-Layer Meteorol* 128(2):205–228
- Webb EK, Pearman GI, Leuning R (1980) Correction of flux measurements for density effects due to heat and water vapour transfer. *QJR Meteorol Soc* 106:85–100. <https://doi.org/10.1002/qj.49710644707>
- Wilson DK (2001) An alternative function for the wind and temperature gradients in unstable surface layers. *Boundary-Layer Meteorol* 99(1):151–158
- Wyngaard J (1984) Boundary-layer modeling. In: *Atmospheric turbulence and air pollution modelling*, Springer, pp 69–106
- Wyngaard J, Coté O (1971) The budgets of turbulent kinetic energy and temperature variance in the atmospheric surface layer. *J Atmos Sci* 28(2):190–201
- Wyngaard JC (1985) Structure of the planetary boundary layer and implications for its modeling. *J Clim Appl Meteorol* 24(11):1131–1142
- Wyngaard JC (2010) *Turbulence in the atmosphere*. Cambridge University Press, Cambridge
- Yamamoto G (1959) Theory of turbulent transfer in non-neutral conditions. *J Meteorol Soc Jpn Ser II* 37(2):60–70
- Yokoyama O (1962) On the contradiction and modification of the equation of diabatic wind profile. *J Meteorol Soc Jpn Ser II* 40(6):359–360
- Zhang Y, Gao Z, Li D, Li Y, Zhang N, Zhao X, Chen J (2014) On the computation of planetary boundary-layer height using the bulk Richardson number method. *Geosci Model Dev* 7(6):2599–2611
- Zilitinkevich S, Gryanik VM, Lykossov V, Mironov D (1999) Third-order transport and nonlocal turbulence closures for convective boundary layers. *J Atmos Sci* 56(19):3463–3477